ACS APPLIED MATERIALS & INTERFACES

Research Article

www.acsami.org

Carbon-Wrapped Fe_3O_4 Nanoparticle Films Grown on Nickel Foam as Binder-Free Anodes for High-Rate and Long-Life Lithium Storage

Dan Li, Xiuwan Li, Suiyan Wang, Yunxian Zheng, Li Qiao, and Deyan He*

School of Physical Science and Technology, and Key Laboratory for Magnetism and Magnetic Materials of the Ministry of Education, Lanzhou University, Lanzhou 730000, China

ABSTRACT: Carbon-wrapped Fe_3O_4 nanoparticle films on nickel foam were simply prepared by a hydrothermal synthesis with sucrose as a precursor of subsequent carbonization. The as-prepared samples were directly used as binder-free anodes for lithium-ion batteries which exhibited enhanced rate performance and excellent cyclability. A reversible capacity of 543 mA h g^{-1} was delivered at a current density as high as 10 C after more than 2000 cycles. The superior electrochemical performance can be attributed to the formation of a thin carbon layer which constructs a 3D network structure enwrapping the nanosized Fe_3O_4 particles. Such an architecture can facilitate the electron transfer and accommodate the volume change of the active materials during discharge/charge cycling.

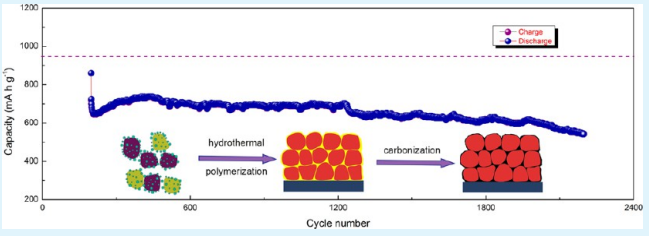

KEYWORDS: *Fe_3O_4 nanoparticles, carbon-wrapping, hydrothermal process, enhanced rate performance, lithium ion battery*

INTRODUCTION

Attention to the development of lithium-ion batteries (LIBs) with high energy density, excellent rate capability, and long cycling life has increased considerably because of the increasing demands for portable electronic devices and electric vehicles (EVs).[1−4] Owing to their relatively low theoretical capacity, traditional graphite-based materials restrict the application of the rechargeable LIBs to the high-power devices.[5,6] As an anode material of LIBs, Fe_3O_4 has been widely investigated with advantages such as higher theoretical capacity (926 mA h g^{-1}), natural abundance, and environmental friendliness. However, large volume change, easy particle aggregation, and low electronic conductivity commonly result in a rapid fading of the capacities during discharge/charge cycling for Fe_3O_4 anodes.[7−9] Enormous efforts have been made to alleviate these problems. One effective approach is to fabricate nanostructured Fe_3O_4, which can provide shorter ion and electron transport pathways, larger electrode/electrolyte contact area, and better accommodation of the strain caused by lithiation or delithiation.[7−12] Another way is to prepare the composites of Fe_3O_4 and carbon, which could not only enhance electronic conductivity but also effectively suppress the large volume expansion during cycling, thus improving the electrochemical performance of the anodes.[13−16]

For preparation of the casted LIB electrodes, adhesives and conductive agents are essential to make the active materials adhere tightly to current collectors and improve the electrical conductivity of electrodes. However, neither the adhesives nor the conductive agents have capacity, reducing the capacity of the electrodes. The preparation of binder- and conductive agent-free electrodes make it possible for obtaining excellent rate capability as a result of the better electrical contacts between the active materials and the used current collectors.[16,17]

In this work, we reported a facile and green approach to prepare binder-free electrodes of carbon-wrapped Fe_3O_4 nanoparticle films on Ni foam for LIBs. It was shown that the synthesized material can perform an excellent rate capability and cyclability. A high specific capacity up to 543 mA h g^{-1} was delivered at a rate as high as 10 C after more than 2000 cycles.

EXPERIMENTAL SECTION

Synthesis of the Samples. Carbon-wrapped Fe_3O_4 nanoparticle films were prepared by a simple hydrothermal process and subsequent carbonization. In a typical procedure, Ni foam (100 PPI pore size, 380 g m^{-2} areal density, and 1.5 mm thick) was first cleaned in an ultrasonic bath with absolute acetone and then dried in a vacuum oven at 60 °C for 10 h. $FeSO_4{\cdot}7H_2O$ (0.27 g, 1 mmol) and sucrose (0.34 g, 1 mmol) were added into 35 mL deionized water and stirred until completely dissolved, and then 1 mL of ammonia (25−28 wt %) was added. The resulting solution as well as the cleaned Ni foam were transferred into a Teflon-lined stainless autoclave with a capacity of 50 mL and kept at 130 °C for 2 h. The product was washed with deionized water and absolute ethanol several times and dried at 80 °C. Finally, it was heat-treated at 600 °C in an argon-flowing tube furnace for 1 h to accomplish the sucrose carbonization.

The masses of the Ni foam and the sample were weighed using a microbalance (Mettler, XS105DU) with an accuracy of 0.01 mg. The active mass of the carbon-wrapped Fe_3O_4 was determined by subtracting the Ni foam mass from the sample mass. The areal density of the active material is about 0.5 mg cm^{-2}.

Hydrothermal synthesis of the Fe_3O_4 nanoparticles can be understood as following well-known chemical reactions:[18,19]

Received: October 27, 2013
Accepted: December 9, 2013
Published: December 9, 2013

Scheme 1. Schematic Illustration Showing the Synthetic Process of the Carbon-Wrapped Fe_3O_4 Nanoparticle Film on Ni Foam

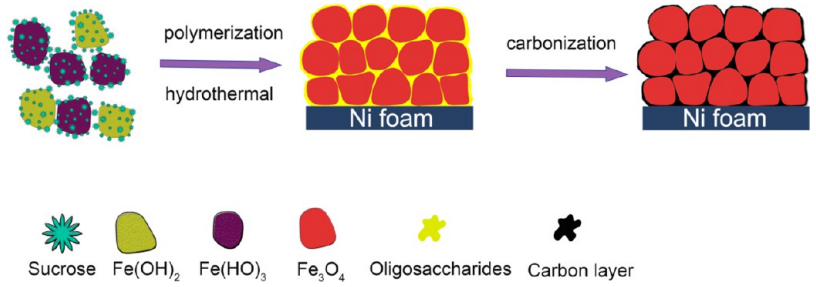

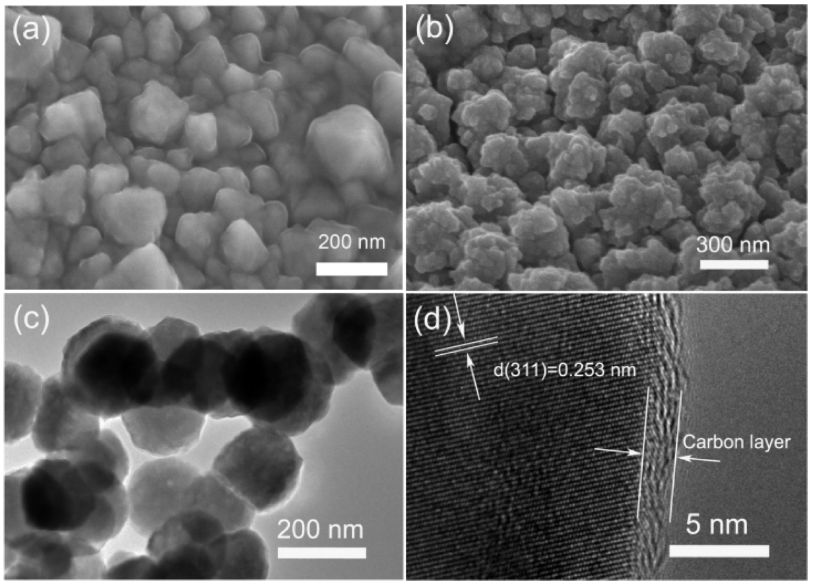

Figure 1. SEM images of the sample (a) before and (b) after heat treatment. (c) TEM image of the nanoparticles scraped from a heat-treated sample. (d) High-resolution TEM image of a single nanoparticle.

$$Fe^{2+} + 2(OH)^- \xrightarrow{pH\ 7-10} Fe(OH)_2 \quad (1)$$

$$4Fe(OH)_2 + O_2 + 2H_2O \xrightarrow{pH\ 7-10} 4Fe(OH)_3 \quad (2)$$

$$2Fe(OH)_3 + Fe(OH)_2 \xrightarrow{130\ ^\circ C} Fe_3O_4 + 4H_2O \quad (3)$$

During the hydrothermal process, the sucrose aggregates into oligosaccharide.[20] The formed Fe_3O_4 nanoparticles are wrapped by the oligosaccharide which structures an interconnected network. In the subsequent heat-treating, the oligosaccharide is transformed into carbon, surrounding the Fe_3O_4 nanoparticles. The schematic diagram of the mentioned synthetic process is shown in Scheme 1. The formed interconnected carbon layer can enhance the electronic conductivity and improve the structure stability of the electrode, and thus the excellent electrochemical performance could be expected for the obtained films as anodes of LIBs.

Structural Characterization. The crystal structures of the resultant materials and the used Ni foam were characterized by X-ray powder diffraction (XRD, Rigaku D/Max-2400, Cu Kα radiation, λ = 0.15418 nm) with a 2θ range from 10° to 90° and a micro-Raman spectrometer (Jobin-Yvon LabRAM HR800 UV) with a radiation of 532 nm. The morphologies were observed using field-emission scanning electron microscopy (SEM, Hitachi S-4800) and transmission electron microscopy (TEM, FEI Tecnai G2 F30).

Electrochemical Characterization. The electrochemical measurements were performed using CR-2032 coin cells. The cells were assembled in a high-purity argon filled glovebox (H_2O < 0.5 ppm, O_2 < 0.5 ppm, MBraun, Unilab) by using the carbon-wrapped Fe_3O_4 nanoparticle films grown on Ni foam as the working electrodes and lithium foil as the counter and reference electrodes. Celgard 2320 was used as the separator membrane. The electrolyte was 1 M $LiPF_6$ dissolved in a mixture of ethylene carbonate (EC), diethyl carbonate (DEC), and ethyl methyl carbonate (EMC) in a 1:1:1 volume ratio. The galvanostatic discharge/charge cycling and cyclic voltammetry measurements were carried out at room temperature by using a multichannel battery tester (Neware BTS-610) and an electrochemical workstation (CHI 660C).

RESULTS AND DISCUSSION

The morphology and microstructure of the carbon-wrapped Fe_3O_4 nanoparticle films on Ni foam were observed by SEM and TEM measurements. Figure 1a shows an SEM image for an as-synthesized sample by hydrothermal process. It can be seen that the film on Ni foam consists of nanoparticles with a smooth surface because the nanoparticles are wrapped with a thin layer of colloidal oligosaccharide. After being heat-treated at 600 °C, the surface of the nanoparticles becomes rough (Figure 1b), and the porous structure can be observed as a result of decomposition and carbonization of the oligosaccharide layer during heat-treating. TEM image of the material scraped from the heat-treated sample as shown in Figure 1c confirms that the sample is composed of the cross-linked nanoparticles. The particles are supposed to be linked together through the carbon layer. On the basis of the high-resolution TEM image of a nanoparticle shown in Figure 1d, the lattice spacing is about 0.253 nm, which is in good agreement with the (311) interplanar distance of Fe_3O_4. More importantly, the single Fe_3O_4 nanoparticle is wrapped by a thin layer of carbon

dx.doi.org/10.1021/am404756h | ACS Appl. Mater. Interfaces 2014, 6, 648−654

and shows a clear core−shell structure. Such a cross-linked morphology of the carbon-wrapped nanoparticles can reduce the particle-to-particle interface resistance by building continuous conductive paths and accommodating the volume change of the Fe_3O_4 nanoparticles when the architecture is used as anodes of LIBs. It is notable that there is not any Fe_3O_4 nanoparticle peeled from the Ni foam after ultrasonic treatment for 3 h, which demonstrates that the active material of the carbon-wrapped Fe_3O_4 nanoparticles and the current collector of Ni foam have an excellent physical adhesive.

In order to confirm the crystal structures and phase components of the samples, XRD measurements were carried out. The scraped materials were used with the avoidance of the diffraction from the used Ni foam. As shown in Figure 2a, all

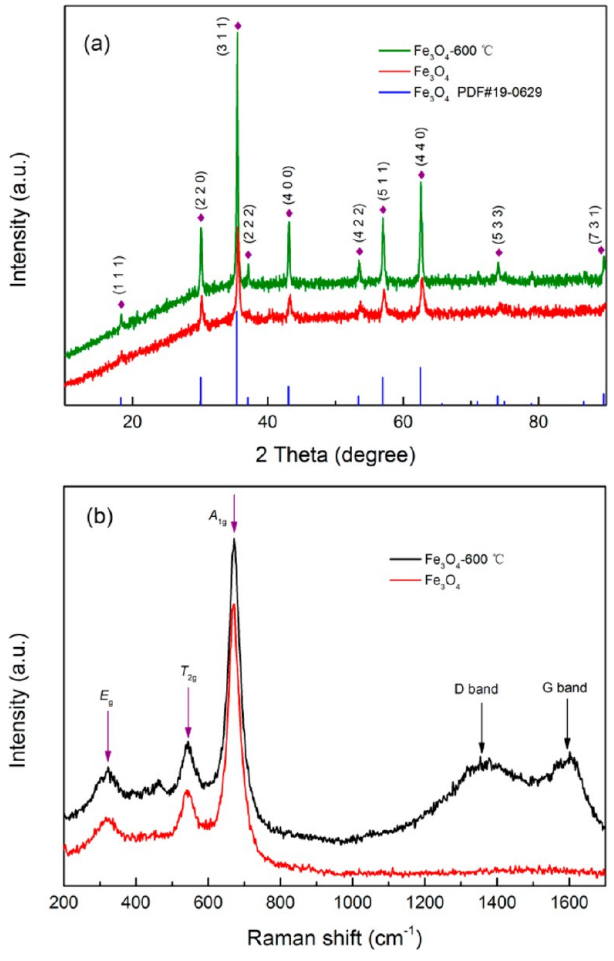

Figure 2. (a) XRD patterns and (b) Raman spectra of the carbon-wrapped Fe_3O_4 nanoparticles scraped from Ni foam before and after heat treatment.

the diffraction peaks before and after the sample being heat-treated in Ar are in good accordance with those of magnetite Fe_3O_4 (JCPDS 19−0629). The peaks at 30.1°, 35.5°, 43.1°, 53.4°, 56.9°, and 62.5° can be indexed to the (220), (311), (400), (422), (511), and (440) crystal planes, respectively. The higher crystallinity for the heat-treated sample is confirmed by the enhanced peak intensity and the additional appearance of the peaks from (111), (533), (444), and (731) crystal plane diffractions. Additionally, no signals related to carbon material were detected because the carbon wrapping is very thin.

Raman spectrum measurement was used to obtain more information about the phase component of the samples. As shown in Figure 2b, the major peaks located at around 326, 537, and 670 cm^{-1} were typical Raman peaks of magnetite Fe_3O_4, which can be assigned to E_g, T_{2g}, and A_{1g} modes, respectively.[21,22] There is a weak peak at about 460 cm^{-1} for the heat-treated sample, which may be an indication of the presence of γ-Fe_2O_3.[23] No Raman peak of carbon appears for the sample before the heat treatment, whereas the typical D peak for disordered carbon and G peak for graphite carbon can be observed for the heat-treated sample,[13,24] suggesting the formation of the carbon layer on the nanoparticles after carbonization.

To investigate the electrochemical characteristics of the carbon-wrapped Fe_3O_4 nanoparticle films on Ni foam, a series of electrochemical evaluations were carried out based on the assembled coin cells with a metallic lithium foil as the counter electrode. The cells were first tested at a current density of 1 C (1 C is defined as 1000 mA g^{-1} to facilitate experimental parameter setting). As shown in Figure 3a, the initial discharge and charge capacities are 1279 and 1009 mA h g^{-1}, respectively, and the corresponding Coulombic efficiency is 79%. The capacity of the electrode exhibits a gradual increase after a dozen cycles, and the Coulombic efficiency is above 99% in the subsequent cycles. A similar capacity increment phenomenon has been widely referred to in the transition metal oxide electrodes, such as hierarchically porous Fe_2O_3 microspheres,[25,26] α-Fe_2O_3/C nanocomposite,[27] Co-based compounds, and CoO anode materials.[28] The most common explanation is due to the reversible growth of a polymeric gel-like film (PGF), which is caused by the decomposition of electrolytes on the surface of the progressively pulverized particles resulting from electrochemical grinding effect.

Cyclic voltammetric (CV) profiles were recorded for the initial three cycles in the voltage range of 0.02−3.0 V at a scan rate of 0.1 mV s^{-1}. As shown in Figure 3b, in the first cycle, the large cathodic peak at 0.52 V corresponds to the reduction of Fe^{3+} and Fe^{2+} to Fe^0, as well as the formation of the solid electrolyte interface (SEI) layer. At the anodic scan, the peak at 1.64 V can be attributed to the reversible oxidation of Fe^0 to $Fe^{2+}$and Fe^{3+}. Due to the polarization of the active Fe_3O_4 nanoparticles in the first cycle, both cathodic and anodic peaks are positively shifted, and the peak at 0.96 V in the cathodic process and the multiple anodic peaks between 1.69 and 1.94 V are observed in the subsequent cycles.[8] The CV curves were found to be well overlapped after the first cycle, indicating the good electrochemical reversibility of the carbon-wrapped Fe_3O_4 nanoparticle film electrode. The electrochemical reaction involved in the cyclings can be described as follows:[29]

$$Fe_3O_4 + xLi^+ + xe^- \rightarrow Li_xFe_3O_4 \quad (4)$$

$$Li_xFe_3O_4 + (8 - x)Li^+ + (8 - x)e^- \rightarrow 4Li_2O + 3Fe \quad (5)$$

$$3Fe + 4Li_2O \rightarrow Li_xFe_3O_4 + (8 - x)Li^+ + (8 - x)e^- \quad (6)$$

$$Li_xFe_3O_4 + xe^- \rightarrow xLi + Fe_3O_4 + xe^- \quad (7)$$

The CV curve of the electrode after 150 cycles is shown in Figure 3c. The redox peaks at 0.62 and 1.51 V deviating from the corresponding peaks appear in the initial cycles shown in Figure 3b, which should be related to the formation of the

dx.doi.org/10.1021/am404756h | ACS Appl. Mater. Interfaces 2014, 6, 648−654

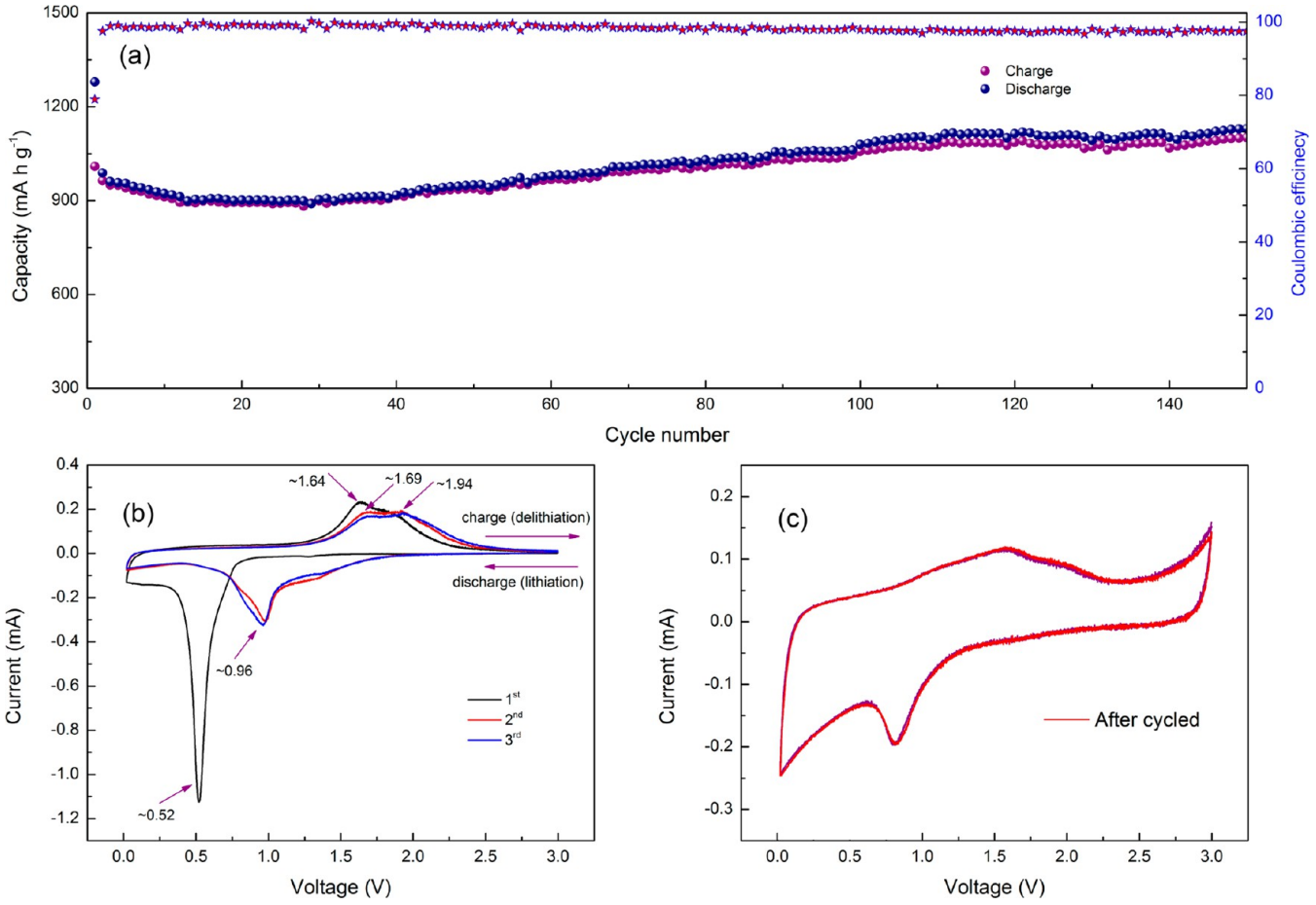

Figure 3. Electrochemical performance of the carbon-wrapped Fe_3O_4 nanoparticle film electrode: (a) Cyclic test of the electrode at 1 C; (b) cyclic voltammograms of the electrode for the initial three cycles; (c) cyclic voltammograms of the electrode after 150 cycles.

stable lithium channel after hundreds of cycles and the polarization of the electrode caused by PGF. In addition, two peaks, which do not appear in the initial cycles, are observed around 0.02 and 3.0 V. This phenomenon can be attributed to the growth of PGF, which may appear at low potentials and disappear at high potentials.[16,30,31] The result is consistent with the capacity increment shown in Figure 3a, and a further explanation will be given later.

The rate capability of the carbon-wrapped Fe_3O_4 nanoparticle film electrode was tested and shown in Figure 4a. It can be seen that the electrode exhibits excellent rate performance. As the current density increases from 0.2 to 0.5, 1, 2, and 5 C, the corresponding specific capacities are 1027, 879, 779, 649, and 507 mA h g^{-1}. Remarkably, the specific capacity can recover to 1092 mA h g^{-1} as the current density returns to 0.2 C. Along with the discharge/charge cycling of the cell, the capacity increases gradually to 1487 mA h g^{-1} in the 197th cycle. The capacity increment is caused by the formed PGF on the surface of the progressively pulverized Fe_3O_4 nanoparticles as mentioned above. The inset in Figure 4a shows the selected discharge/charge voltage profiles, which correspond to the second, 12th, 22nd, 32nd, and 42nd cycles shown in Figure 4a. It can be seen that the electrode exhibits an extended voltage plateau at about 1.0 V in the second discharge, and the charge plateau locates at about 1.7 V in the subsequent cycles, which are well in agreement with the CV profiles shown in Figure 3b. With increasing the rate, the discharge potential decreases and the charge potential increases, which are due to the kinetic effects of the material.[10] Meanwhile, the electrochemical performance of the carbon-wrapped Fe_3O_4 nanoparticle film electrode was evaluated at a low discharge rate of 0.2 C and a high charge rate of 5 C to confirm the excellent rate capability and match the possible application of the electrode. As shown in Figure 4b, the first discharge and charge capacities are 1461 and 896 mA h g^{-1}, respectively, and the corresponding Coulombic efficiency is 61.3%. With gradually decreasing to 661 mA h g^{-1} in the initial dozens of cycles, the discharge capacity can steadily reach 657 mA h g^{-1}, and the Coulombic efficiency is above 95% from the fifth cycle. Such a performance demonstrates that the lithium ion can be quickly released from the lithiated Fe_3O_4 nanoparticles.

To further demonstrate the superior cycling stability of the carbon-wrapped Fe_3O_4 nanoparticle film electrode, the cell after the rate performance test was characterized by the galvanostatic discharge/charge cycling at a rate of 10 C up to 2000 cycles. It is worth noting from Figure 4c that the reversible capacity at a rate of 10 C is higher than that at a rate of 5 C, which can be attributed to the electrochemical activation process of the electrode material. The discharge/charge cycling at high current density leads to the nanocrystallization of the active material, the suppression of the activated nanoparticle aggregation, and the more polymeric gel-like film formation.[32] In the subsequent discharge/charge cycles, the reversible capacity almost stabilized around 543 mA h g^{-1}.

To understand the capacity increment with cycling more clearly, the cell after 380 cycles was disassembled and the cycled

dx.doi.org/10.1021/am404756h | ACS Appl. Mater. Interfaces 2014, 6, 648−654

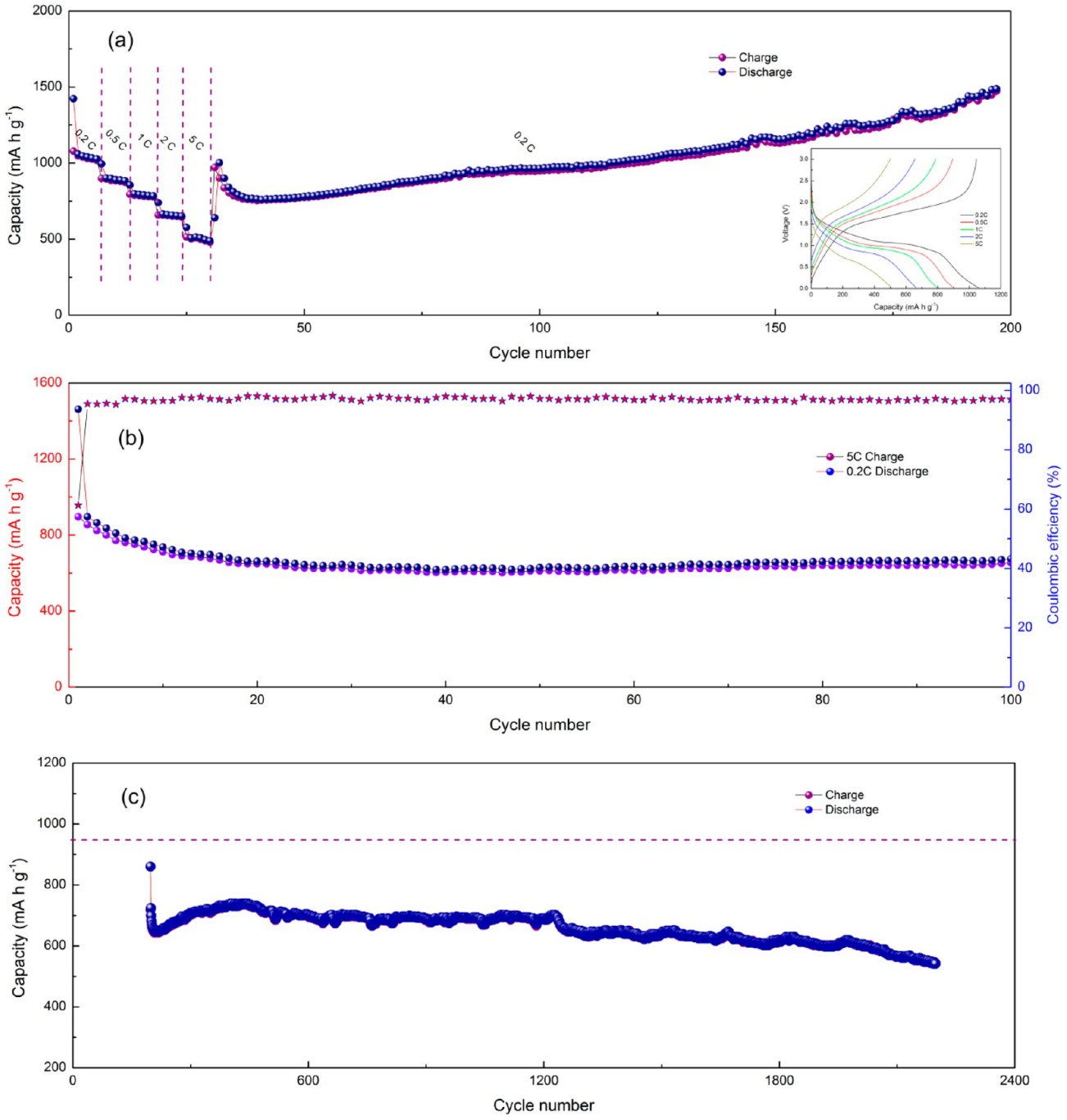

Figure 4. (a) Rate performance of the carbon-wrapped Fe_3O_4 nanoparticle film electrode at current densities of 0.2, 0.5, 1, 2, and 5 C in the voltage range of 0.02−3.0 V. The inset is the selected discharge/charge voltage profiles. (b) Plot of specific capacity vs cycle number at a discharge rate of 0.2 C and a charge rate of 5 C. (c) Subsequent cyclic test of the sample shown in a at a current density as high as 10 C.

Fe_3O_4 electrode was examined by SEM and TEM observations. As shown in Figure 5a, comparing with the morphology of the as-prepared sample shown in Figure 1b, the material becomes more porous, which may greatly increase the electrode/electrolyte contact area and facilitate the insertion/extraction of lithium ions. Figure 5b shows a high-magnification TEM image near a nanoparticle surface. Obviously, some layered materials have been formed on the nanoparticle, and the lattice structure of Fe_3O_4 cannot be observed, which is supposed to be the grown PGF during discharge/charge cycles. The cross-section SEM image of the electrode after 380 cycles is shown in Figure 5c. It can be seen that with the insertion/extraction of lithium ions, the thickness of the carbon-wrapped Fe_3O_4 nanoparticle film increases to more than 3 times compared to the as-prepared sample (Figure 5d). However, the film still keeps its interconnected structure. Due to the increase of the electrode surface area, the electrode/electrolyte contact area increases, making the active material reaction more thorough. In a word, the dramatic change in electrode surface morphology after discharge/charge cycles explains why the capacity increases with cycling and the electrode shows long life performance.

The electrochemical properties of the carbon-wrapped Fe_3O_4 nanoparticle films prepared in the present work and those of

dx.doi.org/10.1021/am404756h | ACS Appl. Mater. Interfaces 2014, 6, 648−654

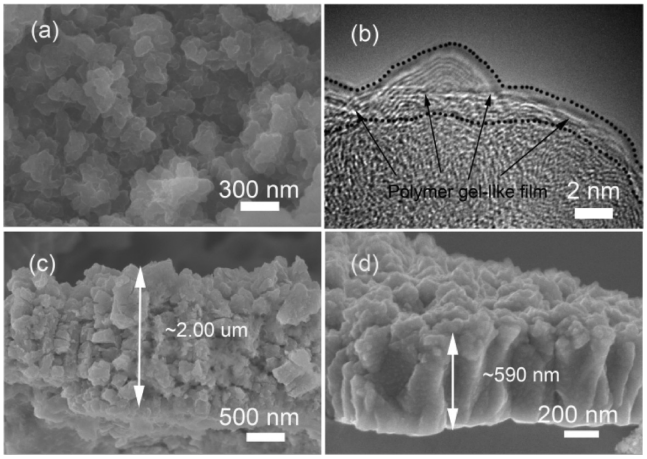

Figure 5. (a) SEM, (b) high-magnification TEM, and (c) cross-sectional SEM images of the carbon-wrapped Fe_3O_4 nanoparticle film electrode after 380 cycles. (d) Cross-sectional SEM image of the as-prepared sample.

the iron oxide materials reported in the literature are summarized in Table 1. It can be seen that the carbon-wrapped Fe_3O_4 nanoparticle film electrode is of excellent high-rate cycling performance.

Table 1. Comparison of the Electrochemical Performance for the Iron Oxides As Anode Materials of LIBs in the Recently Reported Literature

materials	current density	charge capacity after cycling	ref.
Fe_3O_4@C	10 C after rate performance	543 mA h g^{-1} (2197 cycles in total)	this work
Fe_3O_4/C	1848 mA g^{-1}	670 mA h g^{-1} (400 cycles)	24
Fe_2O_3	100 mA g^{-1}	705 mA h g^{-1} (430 cycles)	25
Fe_2O_3/CA	100 mA g^{-1}	408 mA h g^{-1} (500 cycles)	33
α-Fe_2O_3 nanotubes	0.5 C	1000 mA h g^{-1} (50 cycles)	34
Fe_2O_3/Fc@SWCNTs	1300 mA g^{-1}	460 mA h g^{-1} (650 cycles)	35
Fe_2O_3/GNS	1000 mA g^{-1}	~770 mA h g^{-1} (400 cycles)	9
α-Fe_2O_3	1 C after rate performance	nearly 100% capacity retention (800 cycles)	36
α-Fe_2O_3	1 C	910.0 mA h g^{-1} (500 cycles)	16
Fe_3O_4@C@PGC	10 C	only 3.47% capacity loss (350 cycles)	37
α-Fe_2O_3 xerogel	5 C	600 mA h g^{-1} (1000 cycles)	38
C@α-Fe_2O_3@CNT	500 mA g^{-1}	820 mA h g^{-1} (100 cycles)	39

The excellent rate capability and cycling stability of the carbon-wrapped Fe_3O_4 nanoparticle film electrode can be attributed to the following factors. First, the thin carbon layer, which forms a 3D network structure of enwrapped Fe_3O_4 nanoparticles, can facilitate the electron transfer on the electrode/electrolyte interfaces and accommodate the volume change of Fe_3O_4 nanoparticles during the discharge/charge cycling. Second, the carbon-wrapped Fe_3O_4 nanoparticle films directly grown on the Ni foam substrate can form a good adhesion and better electrical contact between the active Fe_3O_4 and the current collector of Ni foam, which is beneficial to providing an efficient electron transport. Third, the small size of the Fe_3O_4 nanoparticles shortens the transport path for both electrons and lithium ions.

CONCLUSION

In summary, we have developed a facile route to grow carbon-wrapped Fe_3O_4 nanoparticle films on Ni foam for high-power LIB applications. The films on Ni foam have better mechanical properties and higher electrical conductivity as anodes, and perform superior lithium storage characteristics with higher capacities, more stable cyclability, and excellent rate capability. Even at a rate as high as 10 C, the capacity higher than 543 mA h g^{-1} was obtained by the galvanostatic discharge/charge test. The experimental results give clear evidence that the carbon-wrapped Fe_3O_4 nanoparticle films on Ni foam can be promising anodes for high-energy and high-power LIBs.

AUTHOR INFORMATION

Corresponding Author

*Tel.: +86-931-8912546. Fax: +86-931-8913554. E-mail: hedy@lzu.edu.cn.

Notes

The authors declare no competing financial interest.

ACKNOWLEDGMENTS

This project was financially supported by the National Natural Science Foundation of China with grant nos. 11179038 and 10974073 and the Specialized Research Fund for the Doctoral Program of Higher Education with grant no. 20120211130005. X.L. Gratefully acknowledges the support of the Fundamental Research Funds for the Central Universities with grant no. lzujbky-2013-232.

REFERENCES

(1) Lou, X. W.; Wang, Y.; Yuan, Ch. L.; Lee, J. Y.; Archer, L. A. *Adv. Mater.* **2006**, *18*, 2325.
(2) Kang, K.; Meng, Y. S.; Bréger, J.; Grey, C. P.; Ceder, G. *Science* **2006**, *311*, 977.
(3) Ni, S.; Zeng, H.; Yang, X. *J. Nanomater.* **2011**, *2011*, 1.
(4) Li, Y.; Tan, B.; Wu, Y. *Nano Lett.* **2007**, *8*, 265.
(5) Scrosati, B.; Hassoun, J.; Sun, Y.-K. *Energy Environ. Sci.* **2011**, *4*, 3287.
(6) Lou, X. W.; Deng, D.; Lee, J. Y.; Feng, J.; Archer, L. A. *Adv. Mater.* **2008**, *20*, 258.
(7) Zhang, J.; Yao, Y.; Huang, T.; Yu, A. *Electrochim. Acta* **2012**, *78*, 502.
(8) Zhang, Q.; Shi, Z.; Deng, Y.; Zheng, J.; Liu, G.; Chen, G. *J. Power Sources* **2012**, *197*, 305.
(9) Zheng, M.; Qiu, D.; Zhao, B.; Ma, L.; Wang, X.; Lin, Z.; Pan, L.; Zheng, Y.; Shi, Y. *RSC Adv.* **2013**, *3*, 699.
(10) Wang, B.; Wu, H. B.; Zhang, L.; Lou, X. W. *Angew. Chem., Int. Ed. Engl.* **2013**, *52*, 4165.
(11) Zhang, L.; Wu, H. B.; Lou, X. W. D. *Adv. Energy. Mater.* 2013, DOI: 10.1002/aenm.201300958.
(12) Chen, J. S.; Zhang, Y.; Lou, X. W. *ACS Appl. Mater. Interfaces* **2011**, *3*, 3276.
(13) Wang, J. Z.; Zhong, C.; Wexler, D.; Idris, N. H.; Wang, Z. X.; Chen, L. Q.; Liu, H. K. *Chem.—Eur. J.* **2011**, *17*, 661.
(14) Zhu, T.; Chen, J. S.; Lou, X. W. *J. Phys. Chem. C* **2011**, *115*, 9814.
(15) Zhang, L.; Wu, H. B.; Madhavi, S.; Hng, H. H.; Lou, X. W. *J. Am. Chem. Soc.* **2012**, *134*, 17388.
(16) Li, X.; Qiao, L.; Li, D.; Wang, X.; Xie, W.; He, D. *J. Mater. Chem. A* **2013**, *1*, 6400.
(17) Wang, X.; Li, X.; Sun, X.; Li, F.; Liu, Q.; Wang, Q.; He, D. *J. Mater. Chem.* **2011**, *21*, 3571.
(18) Li, Y.; Liao, H.; Qian, Y. *Mater. Res. Bull.* **1998**, *36*, 841.
(19) Khollam, Y. B.; Dhage, S. R.; Potdar, H. S.; Deshpande, S. B.; Bakare, P. P.; Kulkarni, S. D.; Date, S. K. *Mater. Lett.* **2002**, *56*, 571.

(20) Wu, X.; Lu, G. Q.; Wang, L. *Energy Environ. Sci.* **2011**, *4*, 3565.
(21) Shebanova, O. N.; Lazor, P. *J. Raman Spectrosc.* **2003**, *34*, 845.
(22) Ni, S.; Wang, X.; Zhou, G.; Yang, F.; Wang, J.; Wang, Q.; He, D. *Mater. Lett.* **2009**, *63*, 2701.
(23) Froment, F.; Tournié, A.; Colomban, P. *J. Raman Spectrosc.* **2008**, *39*, 560.
(24) Yu, Y.; Zhu, Y.; Gong, H.; Ma, Y.; Zhang, X.; Li, N.; Qian, Y. *Electrochim. Acta* **2012**, *83*, 53.
(25) Zhang, J.; Sun, Y.; Yao, Y.; Huang, T.; Yu, A. *J. Power Sources* **2013**, *222*, 59.
(26) Ni, S.; He, D.; Yang, X.; Li, T. *Mater. Chem. Phys.* **2011**, *130*, 1260.
(27) Hassan, M. F.; Rahman, M. M.; Guo, Z. P.; Chen, Z. X.; Liu, H. K. *Electrochim. Acta* **2010**, *55*, 5006.
(28) Sun, Y.; Du, C.; Feng, X.-Y.; Yu, Y.; Lieberwirth, I.; Chen, C.-H. *Appl. Surf. Sci.* **2012**, *259*, 769.
(29) Saadat, S.; Zhu, J.; Sim, D. H.; Hng, H. H.; Yazami, R.; Yan, Q. *J. Mater. Chem. A* **2013**, *1*, 8672.
(30) Ponrouch, A.; Palacín, M. R. *J. Power Sources* **2012**, *212*, 233.
(31) Do, J.-S.; Weng, C.-H. *J. Power Sources* **2005**, *146*, 482.
(32) Ni, S.; Lv, X.; Li, T.; Yang, X.; Zhang, L. *Electrochim. Acta* **2013**, *109*, 419.
(33) Liu, N.; Shen, J.; Liu, D. *Electrochim. Acta* **2013**, *97*, 271.
(34) Wang, Z.; Luan, D.; Madhavi, S.; Li, C. M.; Lou, X. W. *Chem. Commun. (Cambridge)* **2011**, *47*, 8061.
(35) Li, J.; Zhao, Y.; Ding, Y.; Guan, L. *RSC Adv.* **2012**, *2*, 4205.
(36) Hariharan, S.; Ramar, V.; Joshi, S. P.; Balaya, P. *RSC Adv.* **2013**, *3*, 6386.
(37) He, C.; Wu, S.; Zhao, N.; Shi, C.; Liu, E.; Li, J. *ACS Nano* **2013**, *7*, 4459.
(38) Jia, X.; Chen, J.; Xu, J.; Shi, Y.; Fan, Y.; Zheng, M.; Dong, Q. *Chem. Commun. (Cambridge)* **2012**, *48*, 7410.
(39) Wang, Z.; Luan, D.; Madhavi, S.; Hu, Y.; Lou, X. W. *Energy Environ. Sci.* **2012**, *5*, 5252.